The Journal of Experimental Biology 215, 3693-3702

doi:10.1242/jeb.062018

RESEARCH ARTICLE

Ontogeny of aerodynamics in mallards: comparative performance and developmental implications

Terry R. Dial[1,*], Ashley M. Heers[2] and Bret W. Tobalske[2]

[1]Department of Biology, University of Utah, Salt Lake City, UT 84102, USA and [2]Field Research Station at Fort Missoula, Division of Biological Sciences, University of Montana, Missoula, MT 59812, USA

*Author for correspondence (terry_dial@brown.edu)

SUMMARY

Wing morphology correlates with flight performance and ecology among adult birds, yet the impact of wing development on aerodynamic capacity is not well understood. Recent work using chukar partridge (*Alectoris chukar*), a precocial flier, indicates that peak coefficients of lift and drag (C_L and C_D) and lift-to-drag ratio (C_L:C_D) increase throughout ontogeny and that these patterns correspond with changes in feather microstructure. To begin to place these results in a comparative context that includes variation in life-history strategy, we used a propeller and force-plate model to study aerodynamic force production across a developmental series of the altricial-flying mallard (*Anas platyrhynchos*). We observed the same trend in mallards as reported for chukar in that coefficients of vertical (C_V) and horizontal force (C_H) and C_V:C_H ratio increased with age, and that measures of gross-wing morphology (aspect ratio, camber and porosity) in mallards did not account for intraspecific trends in force production. Rather, feather microstructure (feather unfurling, rachis width, feather asymmetry and barbule overlap) all were positively correlated with peak C_V:C_H. Throughout ontogeny, mallard primary feathers became stiffer and less transmissive to air at both macroscale (between individual feathers) and microscale (between barbs/barbules/barbicels) levels. Differences between species were manifest primarily as heterochrony of aerodynamic force development. Chukar wings generated measurable aerodynamic forces early (<8 days), and improved gradually throughout a 100 day ontogenetic period. Mallard wings exhibited delayed aerodynamic force production until just prior to fledging (day 60), and showed dramatic improvement within a condensed 2-week period. These differences in timing may be related to mechanisms of escape used by juveniles, with mallards swimming to safety and chukar flap-running up slopes to take refuge. Future comparative work should test whether the need for early onset of aerodynamic force production in the chukar, compared with delayed, but rapid, change in the mallard wing, leads to a limited repertoire of flight behavior in adult chukar compared with mallards.

Supplementary material available online at http://jeb.biologists.org/cgi/content/full/215/21/3693/DC1

Key words: lift, drag, propeller, flight, bird, ontogeny, life history.

Received 24 June 2011; Accepted 1 July 2012

INTRODUCTION

The avian clade exhibits a broad array of wing morphologies and flight behaviors. Wing morphology varies among species and throughout development, playing a central role in life history and juvenile survival (Dial et al., 2006; Jackson et al., 2009). Although adult morphology correlates with flight performance and ecology (e.g. Rayner, 1988), little is known about aerodynamic function of developing wings, particularly over the range of precocial to altricial birds (Tobalske and Dial, 2007; Heers et al., 2011). Birds that fly early in development are precocial fliers, whereas those that delay flight to adulthood are altricial fliers. The ontogenetic characteristics of feather and wing morphology differ markedly between precocial and altricial fliers (Nice, 1962), such that aerodynamics throughout ontogeny and into adulthood will likely contrast. In this study, we compare the acquisition of aerodynamic lift and drag production in mallards (Anseriformes: *Anas platyrhynchos* Linnaeus 1758; hereafter 'mallard'), which delay flight to the adult stage, with that recently reported for chukar partridges [Galliformes: *Alectoris chukar* (Gray 1830); hereafter 'chukar'], which exhibit early flight capability within 1 week after hatching (Dial et al., 2006; Tobalske and Dial, 2007; Heers et al., 2011).

Wing morphology is reported to affect steady-state aerodynamics during gliding (Withers, 1981). Surprisingly, though, significant changes in wing morphology (planform, leading-edge detail, camber, twist and aspect ratio) appear to have only minor effects upon the aerodynamics of revolving wings, which emulate wing flapping during hovering or flight at very low advance ratios (Usherwood and Ellington, 2002a; Usherwood and Ellington, 2002b; Usherwood, 2009). Among insect and bird wings spanning Reynolds numbers (*Re*) from 1100 in mayfly (*Ephemera vulgata*) to 26,000 in blue-breasted quail (*Conturnix chinensis*), there are no major differences in coefficients of vertical and horizontal force (C_V and C_H, respectively) or, using a frame of reference rotated to account for induced velocities, coefficients of lift (C_L) and drag (C_D) (Usherwood and Ellington, 2002b). Profiles (polar diagrams) of C_V and C_H are also largely unaffected when rock dove (pigeon, *Columba livia*) wings are replaced with flat cardboard replicas (Usherwood, 2009). These results suggest that details of morphology do not significantly affect force production per unit of wing area during hovering or very slow flight. Some exceptions to this pattern, however, include hummingbird (Trochilidae) wings at low angles of attack (α), which produce significantly more lift than flat-plate

models (Altshuler et al., 2004), and recent work with pigeon wings where peak coefficient of lift ($C_{L,max}$) and the lift-to-drag ratio (C_L:C_D) is less with the wing in the posture of upstroke than when in downstroke (Crandell and Tobalske, 2011).

Recently, the ontogenetic development of wing and feather morphology has provided new insight into the relationship between wing design and flapping aerodynamics, at least within the limits of a propeller-force plate model. Heers et al. (Heers et al., 2011) studied a developmental series of chukar and demonstrated that feather properties and microstructure (flexural stiffness, asymmetry, number of barbicels and degree of barbule overlap) all correlate with $C_{L,max}$ and C_L:C_D. In contrast, gross morphology of the wing (camber, aspect ratio and porosity) does not correlate with wing performance across age classes (Heers et al., 2011). This work, performed on the precocially flying chukar, provides a foundation for the present study, in which we conduct an initial comparative test of the generality of the trends reported by Heers et al. (Heers et al., 2011) using mallards, which have an alternative developmental trajectory. Unlike chukars, mallards do not develop a functional wing early in development.

Development of wing function is a crucial component of survival in flying birds, allowing for predator escape and novel foraging opportunities (Jackson et al., 2009). Chukar juveniles, for example, are capable of producing lift within 1 week of hatching as they use their wings to ascend slopes [wing-assisted incline running (WAIR)] (Tobalske and Dial, 2007; Heers et al., 2011) and control aerial descents (Jackson et al., 2009). Their short, broad, highly cambered wings are implemented early in ontogeny for short, accelerative flapping behaviors that allow them to reach a refuge (Dial et al., 2006). At one-fifth the developmental period [20 days post hatching (d.p.h.)], juveniles are capable of sustained flight, and although flight performance improves throughout ontogeny (~100 days), adult flight style changes very little (Dial et al., 2006). In contrast, immature birds of species with altricial wing development, such as the mallard, walk or swim to predator-free refuges. Anseriformes (waterfowl) are precocial in hindlimb-powered locomotion, but delay growth of the forelimbs until just prior to fledging (Stark and Ricklefs, 1998). Waterfowl spend their ontogenetic period exploiting food-rich and predator-free ponds and rivers, using flight at the adult stage for long-distance seasonal migration in addition to burst-escape accelerations that are the hallmark of predator escape in non-migratory chukar (Tobalske and Dial, 2000).

Our goals, therefore, were to explore mallard ontogeny as part of a broader comparative test of the trends reported for chukar (Heers et al., 2011), and to evaluate wing and feather morphology and performance in relation to life-history strategy.

MATERIALS AND METHODS

We generally followed the methods of Heers et al. (Heers et al., 2011) for the experiments and analysis; additional details, particularly regarding the morphology of chukar wings, are available therein.

Wing preparation and ontogenetic series

The mallard ontogenetic series began at 30 d.p.h., whereas the chukar series began at 8 d.p.h. (Heers et al., 2011), as these were the earliest stages of wing development for which our propeller and force-plate apparatus (Crandell and Tobalske, 2011) (supplementary material Fig. S1) could resolve forces when the wings were spun at *in vivo* angular velocities. Wing stages were selected based on transitions in feather morphology and wingbeat kinematics beginning with the emergence of pinfeathers, progressing through barb unfurling, and ending with an adult wing (Tables 1, 2). Two right wings were examined for each ontogenetic stage.

Wings were removed at the shoulder and pinned and taped to dry. The posture of the wings mimicked *in vivo* spread at mid-downstroke, determined using high-speed video (1000 Hz, shutter speed 1/4000 s; Redlake PCI-2000, Redlake, San Diego, CA, USA) of each species during WAIR at 65 deg for chukars (Dial et al., 2008; Jackson et al., 2009) and during descending flight for mallards. These behaviors (WAIR and descending flight) were selected because they could be achieved by birds of all ages. A brass rod (1.5 to 5 mm in diameter according to wing size) was inserted into a pre-drilled hole in the head of the humerus. The attachment was reinforced using epoxy cement. The rod served to mount the wing on the shaft of a motor (see Propeller apparatus and force recordings, below) and provided counterbalance.

Propeller apparatus and force recordings

All wings were mounted ventral side up, with the leading edge of the wing parallel to the horizontal plane of the force plate. The propeller–force-plate assembly was the same for all spin trials (supplementary material Fig. S1) except for the motor used. Mid-experiment, we were compelled to increase the torque capacity of the motor to take the mallard measurements. We used a NEMA 23 brushless DC motor (model BLWR232S-36V-4000, Anaheim Automation, Anaheim, CA, USA; LM3S8971 BLDC motor controller, Luminary Micro, Texas Instruments, Austin, TX, USA) for chukar wings and a NEMA 34 stepper motor (34W214D-LW8; DCL 601USB, MBC 12101 and PSA 40V8A driver and power supply, SMC60WIN v. 2.01 software, Anaheim Automation) for mallard wings.

Table 1. Gross wing morphology and propeller-spin characteristics for different age classes of mallard (*Anas platyrhynchos*)

	Age (days)				
Variable	30	45	50	55	60
Mass (g)	637±71	1028±144	1066±108	1094±4	1208±53
Wing length (cm)	16.9±1.2	31.2±2.0	35.2±1.2	35.9±3.3	39.7±1.7
Wing chord (cm)	3.4±0.1	7.3±1.7	8.1±1.0	6.9±2.7	11.2±0.3
Aspect ratio	5.0±0.2	4.4±1.3	4.4±0.3	5.7±2.7	3.6±0.1
Area (cm^2)	57±6	226±38	285±47	244±76	444±29
Second moment area (m^4)	$4.3\times10^{-5}\pm1.2\times10^{-5}$	$5.4\times10^{-4}\pm4.0\times10^{-5}$	$10.0\times10^{-4}\pm2.9\times10^{-4}$	$8.3\times10^{-4}\pm1.5\times10^{-4}$	$1.8\times10^{-3}\pm2.8\times10^{-4}$
Third moment area (m^5)	$5.0\times10^{-6}\pm1.9\times10^{-6}$	$1.1\times10^{-4}\pm1.8\times10^{-5}$	$2.4\times10^{-4}\pm9.3\times10^{-5}$	$2.0\times10^{-4}\pm2.1\times10^{-5}$	$4.7\times10^{-4}\pm8.5\times10^{-5}$
Porosity (%)	17.3±8.7	5.7±3.4	7.5±3.9	4.7±3.8	4.7±2.6
Camber	0.22±0.06	0.42±0.02	0.45±0.08	0.64±0.01	0.52±0.12
Angular velocity ($rad\,s^{-1}$)	32.5	27.2	28.1	28.1	38.2
Re	11,000±1000	36,000±6000	47,000±8000	40,000±13,000	100,000±7000

See Heers et al. (Heers et al., 2011) for comparable measurements in chukar.

Table 2. Feather microstructure during ontogeny in the mallard (*Anas platyrhynchos*)

Variable	Age (days)				*r*	*P*
	45	50	55	60		
Feather unfurling (%)	74±1	73±9	83±3	99±0	0.91	0.04
Rachis width (% adult)	40±4	49±6	64±15	100±0	0.95	0.02
Feather asymmetry	2.97±0.5	3.89±1.2	4.38±0.1	4.77±0.8	0.97	0.02
Barbicels/barbule	≤1	–	–	1 to 2	0.89	0.15
Barbicel overlap	74±9	–	–	97±12	0.99	0.003

Correlation coefficients (*r*) and *P*-values for peak C_V:C_H as a function of each variable (d.f.=6, except for data from scanning electron micrographs where d.f.=2). For comparable data from chukar, see Heers et al. (Heers et al., 2011).

The motors were attached to a custom-built force plate (Bertec Corporation, Columbus, OH, USA) to measure vertical force and horizontal torque about the *z*-axis (Usherwood, 2009). A shield housing (cowling) isolated the force plate from air velocities induced by upwash from the spinning wing. Resonant frequency for the plate-motor assembly (supplementary material Fig. S1) was 220 Hz. Voltage output from the force plate was amplified (1–100×, depending upon wing size) using a Bertec model M6810 amplifier. Data were imported into a PC using an ADInstruments PowerLab 8SP A/D converter (ADInstruments, Colorado Springs, CO, USA) sampling at 1000 Hz, and recorded using Chart v5.2 (ADInstruments, 1 Hz low-pass digital filter) (supplementary material Fig. S2). Voltages were transformed using known conversions of 10,000 mN V^{-1} for force and 800 mNm V^{-1} for torque.

Spin trials

For each age class, *in vivo* angular velocity, averaged over downstroke (Table 1), was determined using high-speed video and converted to revolutions per minute for driving the propeller (Table 1). We calculated *Re* using average wing chord and wingtip velocity (Ellington, 1984). Angular velocities for chukar were obtained during bouts of 65 deg WAIR (Jackson et al., 2009) and, for mallards, during descending flight. Because of uncertainty on whether such behaviors are directly comparable, we tested intermediate-age chukar and mallard wings at double and half angular velocity. Consistent with Usherwood (Usherwood, 2009), angular velocity did not significantly affect C_V and C_H, particularly over the *in vivo* range of α.

We performed spin trials over a range of α from –20 to 90 deg in ~10 deg increments. Geometrically, α was measured relative to the plane of rotation using reflective markers placed on the feathers overlying the wrist and on the trailing edge of the first secondary. Wings deformed under aerodynamic loading, and herein we report the 'active' α recorded during spinning. Spinning wings were videoed using a Photron FASTCAM SA3 camera (Photron USA, San Diego, CA, USA), with 1024×1024 pixel resolution, sampling at 1000 Hz with a shutter speed of 1/5000 s (Photron PFV v.3.20). We estimate α measurement error at ±1 deg. We used high-speed video frames to calculate change in α (Δα) between 'active' α during spinning and 'static' α prior to spinning.

In an initial attempt to reveal structural mechanisms responsible for ontogenetic changes in morphology and aerodynamic force output, we measured primary-feather stiffness following the methods of Heers et al. (Heers et al., 2011) (seventh primary for day 40 and day 60 birds, *N*=2 for each age class). Here, flexural stiffness (*EI*) was determined as:

$$EI = F_a l^3 / 3\delta, \quad (1)$$

where *E* is Young's modulus, *I* is the second moment of area, F_a is the applied force, *l* is the effective beam length (70% of feather length) and δ is feather displacement (<10% of *l*) (Combes and Daniel, 2003; Vogel, 2003; Heers et al., 2011).

As a check upon our methods, and to further test the functional contribution of feather structure in the juvenile wings, replica chukar and mallard wings were constructed and their aerodynamic properties were evaluated. The flat, artificial wings were made of two pieces of cardboard, glued together using epoxy and reinforced with a 1.4 mm diameter brass rod inserted between the cardboard sheets. Thickness in the region of the rod was 2.08 mm; elsewhere, thickness was 0.68 mm. The wings had the same outline as chukar day 8 and mallard day 30 wings, and the wings were spun at the same angular velocities as appropriate for these two age classes (Table 1). Additionally, C_V:C_H as a function of α was compared against an idealized flat plate without leading-edge suction (i.e. with flow separation). In an idealized flat plate, which has a sharp leading edge and high angle of incidence, aerodynamic force acts perpendicular to the wing surface [C_V:C_H=1/tan(α) (Dickinson, 1996)] as opposed to perpendicular to direction of travel.

Average lift and torque measurements for wings were captured over 10 s of steady-speed rotation (supplementary material Fig. S2). We specifically avoided sampling the transient phases at the start and stop of motor activity, and our plateau phases therefore did not exhibit the same level of transient change as typical of the 'early' or 'steady' phases in Usherwood and Ellington (Usherwood and Ellington, 2002a). The drag produced by the counterbalancing rods during these trials was subtracted (Usherwood, 2009; Heers et al., 2011).

Vertical and horizontal force coefficients (C_V and C_H) were determined from the force-plate output. Vertical force (F_V) was measured directly along the *z*-axis and horizontal force (F_H) was determined from the torque (*Q*; Nm) about the *z*-axis. Force coefficients were calculated from these measures following Usherwood and Ellington (Usherwood and Ellington, 2002a). C_V was calculated as:

$$C_V = 2F_V / \rho S_2 \Omega^2, \quad (2)$$

where ρ is air density (1.07 kg m^{-3} for Missoula, MT, USA), S_2 is the second moment of area (m^4) and Ω is the angular velocity of the wing (rad s^{-1}). C_H was calculated as:

$$C_H = 2Q / \rho S_3 \Omega^2, \quad (3)$$

where S_3 is the third moment of area (m^5). Previous research has included C_L and C_D computed using a rotated frame of reference that takes into account estimated induced velocities at blade elements along the span of the rotating wing (Usherwood and Ellington, 2002a; Usherwood and Ellington, 2002b; Usherwood, 2009; Heers et al., 2011; Crandell and Tobalske, 2011). Because aspect ratio should have an effect upon lift distribution and local induced velocities, aspect ratio may be confounded with C_L and C_D, so for our present comparative analyses we use only C_V and C_H.

For each wing, 100-point spline-interpolation curves were fitted for C_V and C_H *versus* active α (–15 to 80 deg; IGOR Pro v.6.12, Wavemetrics, Portland, OR, USA). We used the fitted curves to compute means for the two wings for each age class. We used the averaged values to produce polar diagrams of C_V as a function of C_H and C_V:C_H as a function of α.

Wing morphology and feather microstructure analysis

We measured aspects of wing morphology [length (m), area (m^2), second and third moments of area (m^4 and m^5) and wing porosity (%) (Heers et al., 2011)] using a digital camera to photograph the dorsal view of a dried wing. We analyzed these images using ImageJ (v1.42, National Institutes of Health, Bethesda, MD, USA) and custom m-files in MATLAB R2010a (The MathWorks, Natick, MA, USA). We determined maximum camber (dimensionless) by dividing maximum wing height at the wrist by average wing chord (Heers et al., 2011). Wing height was measured as the highest point of curvature with the wing set ventral side down on a flat table. Maximum height was consistently at the wrist. Camber values are likely inflated relative to camber for a blade element centered on the wrist due to long-axis curvature of the whole wing, which was not taken into account for the measurement. Aspects of feather microstructure were determined for the mallard at days 45, 60 and post-molt adult. Consistent with Heers et al. (Heers et al., 2011), we removed the 10th primary feather for light scanning (HP Photosmart scanner, Hewlett-Packard, Palo Alto, CA, USA, at a resolution of 236 pixels cm^{-1}) to determine feather unfurling (%), asymmetry (%) and rachis width (mm). The feathers on the wings of day 30 mallards were downy, so quantitative comparisons were not feasible. We obtained scanning electron micrographs (Hitachi S-4700 cold field emission SEM, Hitachi High Technologies America, Pleasanton, CA, USA) at the tip and 25% proximal from the tip of the feather to determine barbule overlap (%) and barbicel/barbule ratios (dimensionless). For further comparison, a post-molt adult feather was obtained from the University of Montana, Philip L. Wright Zoological Museum.

Transmissivity

Based upon morphology of the wings (Heers et al., 2011), we hypothesized that wing transmissivity (Müller and Patone, 1998) would be at least partially responsible for relatively poor aerodynamic performance in juvenile wings. Here we define two scales of transmissivity, or air movement perpendicular to the wing surface, from the underside to the upper side. Macroscale is considered to be air movement between feathers; microscale is considered to be air movement between barbs, barbules and barbicels. We used particle image velocimetry (PIV) (Spedding et al., 2003; Tobalske and Dial, 2007) to measure macroscale transmissivity in mallard wings at days 40 and 60 and our cardboard day 30 model, and we used a vacuum-driven flow circuit (Müller and Patone, 1998) to measure microscale transmissivity in the day 40 and day 60 wings.

Macroscale transmissivity was determined by placing wings in a wind tunnel [for details of the tunnel, see Tobalske et al. (Tobalske

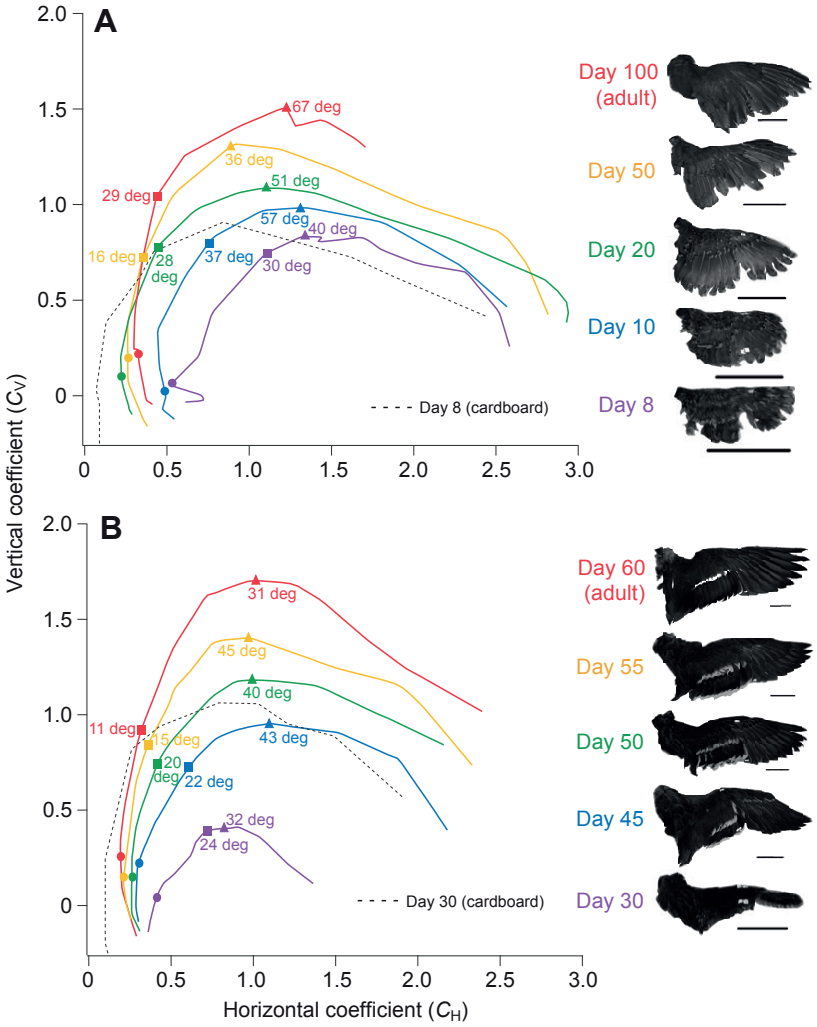

Fig. 1. Polar traces of vertical force coefficient (C_V) and horizontal force coefficient (C_H) for an ontogenetic series coupled with dorsal profiles of wings from (A) chukar partridge (*Alectoris chukar*) and (B) mallard (*Anas platyrhynchos*). C_V and C_H were measured at angles of attack (α) from –15 to 80 deg. Symbols refer to α=0 deg (circles), maximum C_V:C_H (squares; α indicated) and maximum C_V (triangles; α indicated). Axes are the same scale to aid comparison. Solid, colored traces are means from N=2 birds per age class, with classes beginning at the earliest age force readings could be resolved and ending with adult wings. Gray dashed lines are from flat cardboard models of the youngest chukar and mallard (N=1 per species). Scale bars, 5 cm (for wing images).

et al., 2005)] and using PIV to reveal near-field flow about the wing surface (Spedding et al., 2003; Warrick et al., 2005; Tobalske and Dial, 2007; Tobalske et al., 2009). We measured the cardboard wing chord at the blade element two-thirds of the distance from the shoulder to the wingtip; primaries 1–3 were measured in the day 40 and day 60 birds. Wings were placed perpendicular to air flow (α=90 deg). Air speed in the wind tunnel was matched to the wing speed of primaries 1–3 during spinning trials, which meant that free-stream velocity was 3.6, 3.3 and 8.8 m s^{-1} for the cardboard model, day 40 wing and day 60 wing, respectively. We obtained 50 images and averaged velocity to then compute vorticity from the averaged flow field. Our interrogation area for sampling velocity was a square centered on the wing or primaries, with side lengths of the square equal to 75% of the width of the chord (cardboard model and day 40 wing) or the width from the edge of primary 1 to the edge of primary 3 (day 60 wing). The sampled areas were immediately in front of and behind the wing, outside of the shadow created by the wing that obstructed the laser light.

For PIV, we used a LaVision system with DaVis 7.1 software (Goettingen, Germany), a Flowmaster 1376×1040 pixel digital camera (Goettingen, Germany) sampling at 5 Hz and a 50 mJ dual-cavity pulsed Nd:YAG laser (New Wave Research, Fremont, CA, USA). We seeded the air with particles of olive oil (<1 µm in diameter) generated at a rate of 7×10^{10} particles s^{-1} using a vaporizer fitted with a Laskin nozzle. We placed the camera perpendicular to the planar (~3 mm thick) illumination field. To calculate particle velocity, we used cross-correlation of paired images with an elapsed time between images (Δt) of 250–400 ms to give ~10 pixel particle separation in the regions of greatest velocity. We employed an adaptive multipass with an initial interrogation area of 64×64 pixels and final area of 16×16 pixels with 50% overlap. Vector fields were post-processed using a median filter (strong removal if the difference relative to the average was more than two times the r.m.s. of neighbors, and iterative reinsertion if it was less than three times the r.m.s. of neighbors), removal of groups with less than vectors, fill of all empty spaces by interpolation and one pass of 3×3 smoothing. We estimated the minimum error in velocity measurements to be 5.0±0.5% including contributions due to a correlation peak of 0.1 pixels, optical distortion and particle–fluid infidelity (Spedding et al., 2003).

Air movement through an individual feather, defined as microscale transmissivity (T; m^3 s^{-1} N^{-1}), was measured using a closed-line flow circuit, designed to measure the pressure differential across feather sections at the barb–barbule–barbicel level (Müller and Patone, 1998). A Shop-Vac Pro vacuum (Shop-Vac, Williamsport, PA, USA) provided suction in the circuit; flow rate was regulated using a Brooks Flowmeter (1355-00C1 AAA, Emerson Electric, Hatfield, PA, USA) and pressure across the feather was measured using a Setra Datum 2000 Pressure Transducer (2239 Manometer, Setra Systems, Boxborough, MA, USA). Transmissivity was calculated as:

$$T = Q / (\Delta P A), \quad (4)$$

where Q is air flow (1 m^{-2}), ΔP is the pressure differential across the feather section (Pa; 1 Pa=1 N m^{-2}) and A is area (m^2). Transmissivity is therefore a variable describing the degree to which air passes through a section of feather, regardless of the pressure differential or area of feather sample (Müller and Patone, 1998). Feather samples were taken from the inner vane, 10% inward from the feather tip in the second primary of day 40 and day 60 mallards and also in a tertial feather of a day 60 mallard.

Statistical analysis

We tested for correlations between peak C_V:C_H and variables in mallards describing whole-wing morphology using values for each individual within each age class. To describe whole-wing deformation during spin trials, we regressed $\Delta\alpha$ as a function of the resultant force coefficient (C_R=C_v+C_h) using least-squares regression. Statistical analyses were performed using Excel (v.2010, Microsoft, Redmond, WA, USA) and IGOR Pro (v.6.12, Wavemetrics). Throughout, we report means ± s.d. except in graphs, where we report mean and range (i.e. minimum–maximum for N=2 birds per age class).

RESULTS

Mallards reached an average terminal mass of ~1300 g (Dial and Carrier, 2012) over a 60 d.p.h. ontogenetic period, whereas previous work has shown that fully grown chukar average ~600 g and develop for ~100 d.p.h. (Tobalske and Dial, 2000; Dial et al., 2006; Jackson et al., 2009). Peak vertical coefficient ($C_{V,max}$) and maximum C_V:C_H were observed to be roughly similar at comparable stages of development, and a marginally higher peak in the adult mallard compared with the adult chukar appeared insignificant given the large variation between conspecifics in the same age class. Consistent with the patterns previously reported for C_L and C_D in chukar (Heers et al., 2011), mallards exhibited an ontogenetic increase in $C_{V,max}$ and

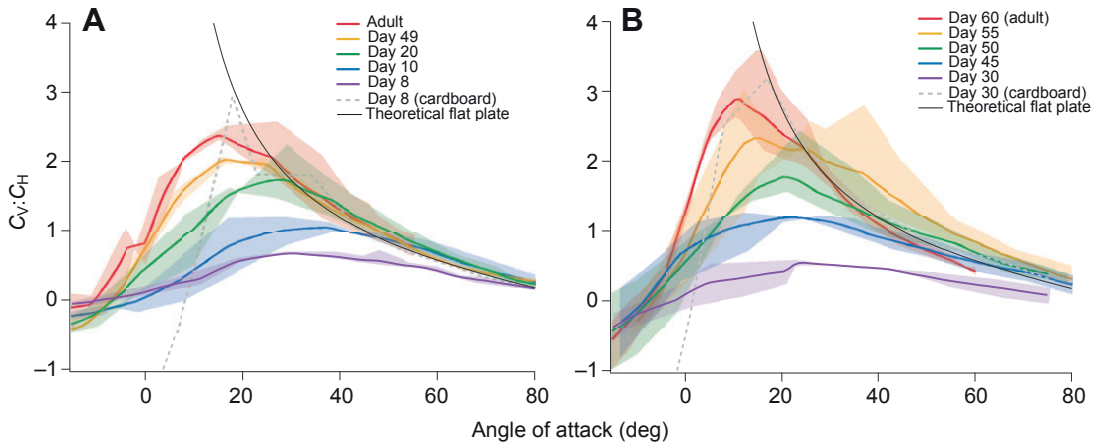

Fig. 2. Lift-to-drag ratio (C_V:C_H) over range of angle of attack (α=–15 to 80 deg) for an ontogenetic series from (A) chukar partridge (*Alectoris chukar*) and (B) mallard (*Anas platyrhynchos*) (N=2 birds per age class). Gray dashed lines are from flat cardboard models of the youngest chukar and mallard (N=1 per species). The solid black line represents theoretical flat plate. Axes are the same scale for comparison between wing types. Lines and their respective shaded regions represent means, minimums and maximums.

C_V:C_H (Figs 1–4). Furthermore, as in Heers et al. (Heers et al., 2011), we observed significant correlations between maximum C_V:C_H and four measures of feather microstructure – feather unfurling, rachis width, feather asymmetry and barbule overlap (Fig. 4, Table 2) – whereas there was no significant effect of camber, aspect ratio or wing porosity ($0.37<P<0.91$; Tables 1, 2).

Comparative aerodynamic performance

In both species, peak C_V:C_H increased with age and was generated at progressively lower α (Figs 1, 2). Day 8 chukar wings produced more horizontal force ('drag') compared with vertical force (maximum C_V:C_H=0.88, α=30), whereas day 10 chukar wings were capable of producing more vertical than horizontal force (maximum C_V:C_H=1.44, α=37 deg; Fig. 1A, Fig. 2A), and by the final stage of chukar wing development (day 100), maximum C_V:C_H increased to 4.0 (Figs 2, 3). Day 30 mallard wings were practically incapable of vertical force generation: even at maximum C_V:C_H, horizontal force outweighed vertical force (C_V:C_H=0.64). Between day 30 and day 45, peak C_V:C_H improved from 0.64 to 1.46. Aerodynamic performance culminated at the adult condition with wings capable of producing maximum C_V:C_H=5, 40% more vertical than horizontal force at α=0 deg (C_V:C_H=1.40), and $C_{V,max}$>2 (at α=31 deg; Fig. 1B, Fig. 4C). It is worth noting that the day 60 mallard has not gone through a molting period, whereas the day 100 chukar has. Post-molt feathers have greater aerodynamic performance in chukar (Heers et al., 2011), suggesting that post-molt feathers in mallards might have even greater performance than that reported here for day 60 birds. *In vivo* wing kinematics (from the initial videos taken to determine wing angular velocities) suggest that α is not optimized for maximum C_V:C_H or $C_{V,max}$, but rather spans a range of α values. Both C_V:C_H and $C_{V,max}$

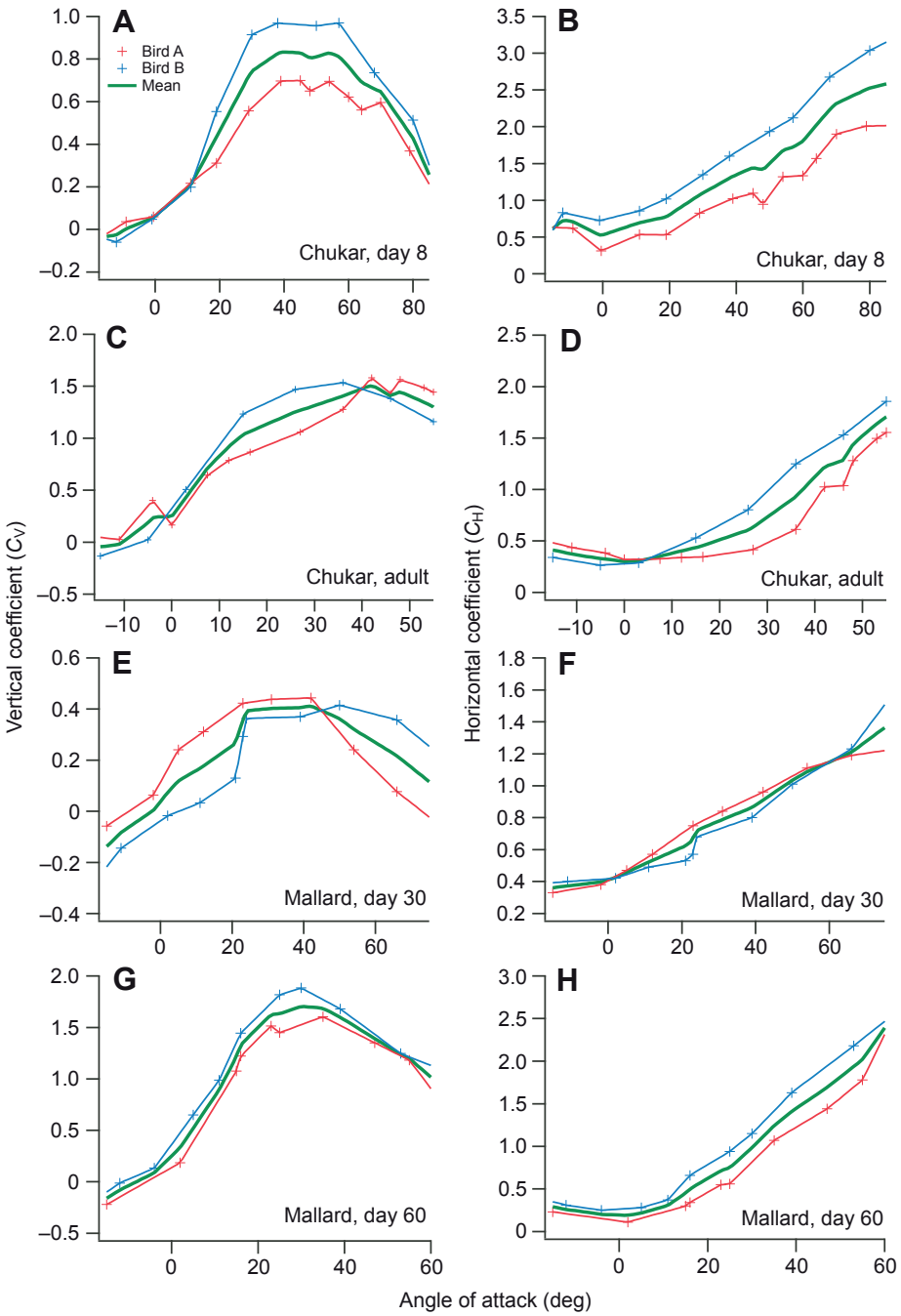

Fig. 3. Variability between wings (N=2 per age class) for coefficient of lift (C_V; left column) and coefficient of drag (C_H; right column) as a function of angle of attack for (A,B) chukar, day 8; (C,D) chukar, adult; (E,F) mallard, day 30; and (G,H) mallard, day 60. Red and blue indicate individual wings; green indicates the mean.

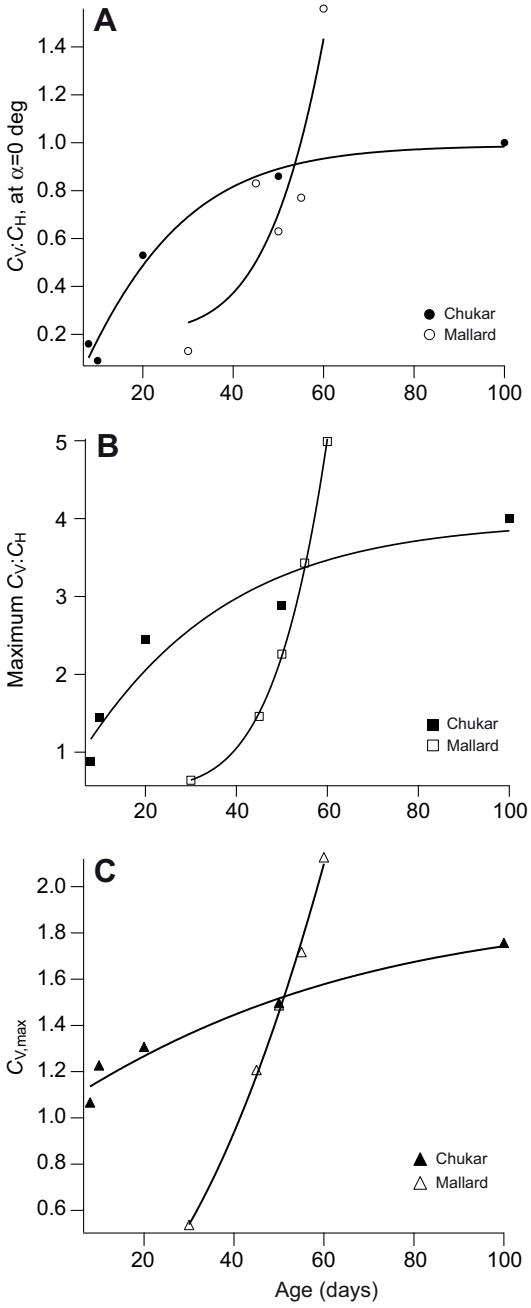

Fig. 4. Ontogenetic trends between chukar and mallards at different points along the polar curves. (A) Change in C_V:C_H at α=0 deg. (B) Maximum C_V:C_H, α indicated in Figs 1, 2. (C) Maximum C_V, α indicated in Fig. 1. Note the characteristic trend that chukar wing function initiates early and gradually improves throughout ontogeny, where mallard aerodynamic capacity is delayed to a brief window of maturation just prior to fledging.

are, therefore, important metrics in comparing aerodynamic performance between species and over the course of ontogeny.

Our cardboard models of 8 day chukar wings and 30 day mallard wings exhibited higher $C_{V,max}$ and peak C_V:C_H as well as lower minimum C_H compared with wings from real birds (Figs 1, 2). For the bird wings, C_V:C_H<1.5, whereas C_V:C_H=3.15 at α=17 deg in the duck cardboard model and C_V:C_H=2.92 at α=18 deg in the chukar cardboard model. Minimum C_H=0.10 (α=8 deg) in the duck cardboard model and 0.07 (α=10 deg) in the chukar cardboard model, whereas C_H~0.5 at α=0 deg in the youngest bird wings (Fig. 1). When compared with a theoretical flat plate (Dickinson, 1996), 50 day wings and older exhibited slightly higher C_V:C_H values when α>15 deg, but differences were generally within the range exhibited between individuals of a given age class (Fig. 2).

Considerable variation was apparent between the two wings within each age class, although this variance was proportionally greater for the wings from the youngest birds and tended to decrease with age (Fig. 3). We attribute this variance to differences in morphology of the dried wings (note the standard deviations in Tables 1, 2), as well as error introduced with the lower signal-to-noise ratio inevitable when measuring smaller forces from the wings of the youngest birds (supplementary material Fig. S2).

A stark contrast was apparent in the timing and trajectory of aerodynamic development between mallards and chukar. Chukar show early, gradual improvements (Heers et al., 2011), whereas mallards show delayed, dramatic shifts in aerodynamic capacity (Fig. 4). The earliest stage at which chukar and mallard wings were capable of producing lift that was measurable with our force-plate apparatus was day 8 and day 30, respectively (Fig. 4). More-sensitive flow measurements reveal that wings from younger (day 4) chukar can generate lift (Heers et al., 2011), but we did not attempt such measurements for mallards in the present study. For chukar, day 8 corresponds well with the *in vivo* onset of lift during controlled flapping descent and WAIR (Tobalske and Dial, 2007; Jackson et al., 2009). However, flapping-descent experiments with mallards (Dial and Carrier, 2012) reveal that they do not produce significant lift *in vivo* until day 45 (supplementary material Fig. S3). From day 8 and day 45, respectively, the time period required to reach the adult-wing condition was 90 days for the chukar and 15 days for the mallard wings (Heers et al., 2011) (Fig. 4).

Feather morphology changed consistently with increasing age in mallards (Table 2, Fig. 5). Feather unfurling increased from 74 to 99%, rachis width (relative to adult condition) increased from 40 to 100%, feather asymmetry increased from 3 to 5, barbicels/barbule increased from ≤1 barbicel to between 1 and 2 barbicels (post-molt adult: >5), and barbule overlap increased from 74 to 97% (post-molt adult: 109±11%). In contrast, although absolute measures of length and area of the wings obviously increased with age (Fig. 1, Table 1), our measures of gross morphology that do not contribute to calculations of C_V and C_H (namely aspect ratio, camber and wing porosity) did not vary in a consistent manner with age in mallards (Table 1, Fig. 1), as previously reported for chukar (Heers et al., 2011).

Flexibility and transmissivity

Our direct measures of flexural stiffness (*EI*) revealed that feather stiffness for primary 2 increased dramatically with age. For day 40 mallard, $EI=9.3\times10^{-5}$ Nm^2 and for day 60, $EI=9.18\times10^{-3}$ Nm^2, indicating that day 60 feathers are much stiffer than day 40 feathers. These values of *EI* were on par with day 20 and day 100 chukar (Heers et al., 2011). Regressing Δα as a function of C_R, we observed that wing and feather deformation during spin trials increased throughout ontogeny ($\Delta\alpha=7.6C_R-7.8$, $r=0.79$, $P<0.01$, d.f.=1,9). Although the older feathers are stiffer, they deformed more during spin trials, likely because of higher C_R. In general, spinning wings deformed under aerodynamic loading by twisting along the long axis such that that the absolute value of α decreased (i.e. negative initial α became less negative; positive initial α became less positive). For example, the average Δα among all subjects and age classes of mallards with an active (spinning) α~45 deg was –4±5 deg relative to the static α.

Macroscale transmissivity decreased throughout ontogeny. Average air velocities perpendicular to the day 40 wing were

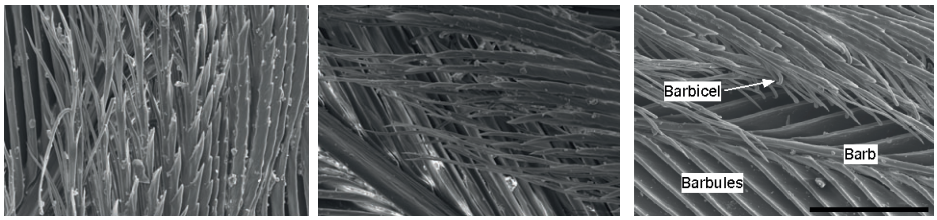

Fig. 5. Ontogenetic trends in mallard feather microstructure. Note the number of barbicel hooklets and overlap between barbules. Scale bar, 100 μm. Images magnified ×500. See Heers et al. (Heers et al., 2011) for comparable images from chukar.

2.5±0.3 m s^{-1} leading into the wing and 1.2±1.3 m s^{-1} behind the wing, indicating that flow passes through the individual feathers and leaves a highly variable flow field behind the wing (Fig. 6). In contrast, flow in the vicinity of the day 60 wing (4.8±1.4 m s^{-1} incurrent and –0.6±0.5 m s^{-1} in the wake) indicates recirculation of air in a vortex-formation region, with feathers acting together like a flat plate (Vogel, 1994). Our actual flat-plate, cardboard replica exhibited a flow pattern and velocity distribution similar to that of the day 60 wing, with incurrent velocity in front of the cardboard wing at 2.1±0.8 m s^{-1} and velocity behind the model at –0.2±0.1 m s^{-1}.

Microscale transmissivity (T) also decreased throughout ontogeny. Within the vacuum-driven flow circuit, average transmissivity at flow rates (Q) >0.49 was 2.6×10^{-4} m^3 s^{-1} N^{-1} for day 40 primary 2 and 1.4×10^{-4} m^3 s^{-1} N^{-1} for day 60 primary 2 (Fig. 7). Smaller numbers indicate that less air passes through the section of feather, so the day 60 primary was much less transmissive than the day 40 primary. For comparison, the day 60 tertial had higher average T than either primary feather: 1.15×10^{-3} m^3 s^{-1} N^{-1}. These values of T in the day 40 and day 60 birds are within the range of values for T reported for feathers in the European kestrel (*Falco tinnunculus*) (Müller and Patone, 1998).

DISCUSSION

The general trends we observed in mallards for the development of aerodynamic forces and feather morphology were consistent with those previously reported for chukar as coefficients of lift and drag (Heers et al., 2011), supporting a conclusion that feather microstructure probably has a more dramatic effect than gross wing morphology upon wing aerodynamics during spinning (Table 2, Fig. 5). Cardboard models with the same outline as juvenile bird wings generated higher $C_{V,max}$ and C_V:C_H, and lower minimum C_H, which further emphasizes the important role of feather structure upon wing performance. Overall, our results are consistent with an interpretation that whole-wing morphology has scant influence upon performance during spinning trials (Usherwood and Ellington, 2002a; Usherwood and Ellington, 2002b; Usherwood, 2009; Heers et al., 2011) unless wing posture is radically altered as during upstroke *versus* downstroke (Crandell and Tobalske, 2011).

Our results support a recommendation that, for take-off and slow flight at low advance ratios, resultant force coefficients (C_R) are appropriately modeled as being perpendicular to the plane of a bird's wing rather than perpendicular to the direction of wing translation (Dickinson, 1996). The expectation for a translating flat plate is that C_R is perpendicular to the plane of the plate when α>15 deg, potentially, but not necessarily, associated with formation of a leading-edge vortex (Dickinson, 1996). Wings from older birds (day 50–60) exhibited slightly higher values of C_V:C_H compared with values for such a theoretical flat-plate model, particularly at 15 deg≤α≤45 deg (Fig. 2), but the high variability between individuals in each age class suggests it is best, at present, to conclude rough agreement with predictions from a flat-plate model.

In addition to corroborating general trends in chukar (Heers et al., 2011), our study offers novel observations about potential aerodynamic mechanisms that can account for the trends as well as new insight into the timing of wing development. Macroscale and microscale transmissivity both decreased with age in mallards (Figs 6, 7). We therefore conclude that stiffer feathers and wing impermeability to air creates a wing capable of generating greater aerodynamic force across a large range of α (Figs 2, 3). This pattern is consistent with data from the fossil record, which suggest that barbules and barbicels [i.e. closed pennaceous feathers (Prum, 1999)] evolved in theropods that were beginning to accumulate skeletal features associated with flight capacity. Feather maintenance (preening) likely functions to realign feather overlap (Clumpner, 1990), as well as interdigitate barbicels (hooklets) at the microscopic level, and thus may be important for reducing transmissivity. As all aspects of development are intercorrelated (Tables 1, 2), a future challenge will be to isolate aspects of feather structure to test the relative contribution of variables such as flexural stiffness or barbule overlap upon macroscale and microscale transmissivity. Likewise, it will be necessary to isolate macroscale and microscale transmissivity to understand their effects upon aerodynamic performance.

The timing of wing development differs dramatically between mallards and chukar (Heers et al., 2011) (Fig. 4). This appears to be due to the mechanisms juveniles use for escape, and it may reflect different selective pressures early in life history. Although precocial in their early locomotor ability to run and swim, the developmental trajectory of the mallard forelimb parallels that of altricial birds. Developing mallards do not use flight for survival during their vulnerable period as juveniles; instead they swim to a refuge. Wing maturation initiates late in ontogeny and is condensed to a brief window of ~15 days (Fig. 4). In contrast, it is likely that strong selective pressures (e.g. predation) have acted historically and are currently acting on terrestrial chukars to cause them to use their wings to produce aerodynamic force prior to attaining mature size. Juvenile chukars beginning at ~7 days will use their wings to produce lift and help them escape as they run up slopes; this is well before they can support their weight in flight (Tobalske and Dial, 2007; Jackson et al., 2009).

Might the differences between species in timing of wing development be related to their adult flight styles? As adults, mallards exhibit impressive capacity for burst take-off, but they are also highly migratory (Cooke, 1933); in contrast, adult chukar use high-power, burst take-off for escape and then immediately return to the ground to run for cover (Tobalske and Dial, 2000).

It has been suggested that an inherent tradeoff exists between the functional maturity of structures and the rate of morphological development (Carrier, 1996; Stark and Ricklefs, 1998). As a result of ontogenetic canalization (Frazzetta, 1975; Carrier, 1996), it may be that wing morphology and aerodynamic capacity in adults is constrained by early onset of aerodynamic function in juveniles. Future research should seek to test this idea in a broader phylogenetic context, as interpretation of two-species comparisons (i.e. mallard *versus*

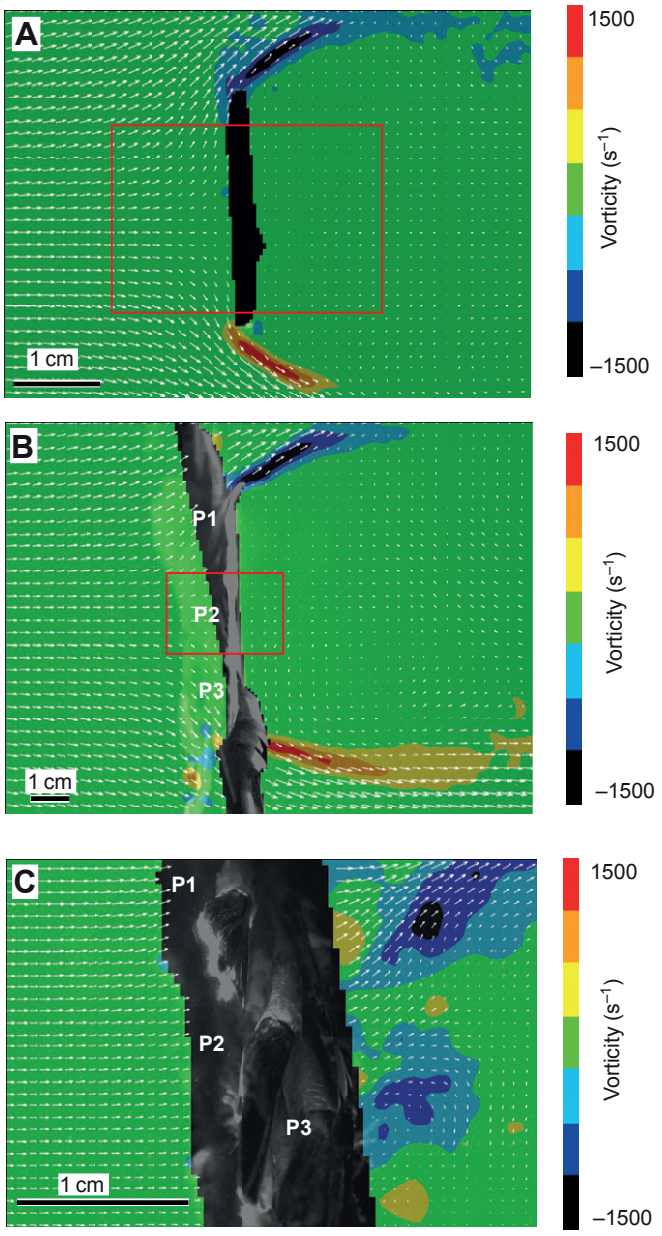

Fig. 6. Macroscale transmissivity in duck wings and a cardboard model as measured using particle image velocimetry. (A) Cardboard model of day 30 wing, with black shading revealing the cross-section of wing. (B) Day 60 wing, with three primaries (P1, P2 and P3) isolated to permit observation of local flow. (C) Day 40 wing, with close view of P1, P2 and P3. Red boxes in A and B indicate comparable size of interrogation area used for C. White vectors represent velocity ($m\,s^{-1}$) and background colors represent vorticity ($rad\,s^{-1}$). Areas in the vicinity of feathers in B and C were masked because shadows caused by other feathers precluded measurements of local velocity.

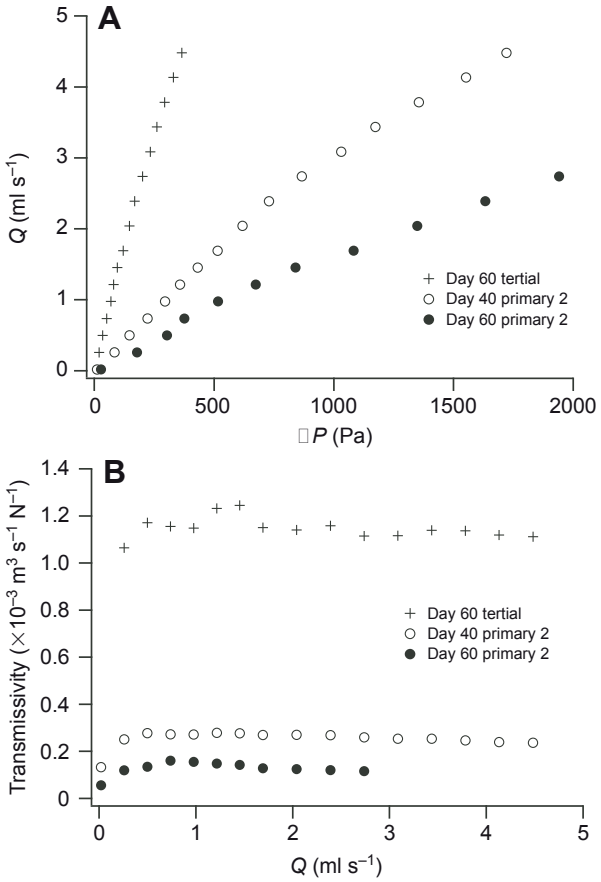

Fig. 7. (A) Microscale transmissivity showing flow rate (Q) as a function of the pressure differential across the feather (ΔP); this is for direct comparison with Müller and Patone's fig. 3 (Müller and Patone, 1998). The slope indicates conductance, and conductance per unit area is transmissivity. (B) Transmissivity as a function of Q.

chukar) necessarily requires extreme caution (Garland and Adolph, 1994) and is inadequate for testing for adaptation or revealing patterns of transformation (Gould and Lewontin, 1979; Lauder, 1981).

The Galliformes may be an excellent phylogeny within which to test the 'canalization' hypothesis that early life history has driven adult morphology and behavioral repertoire. Some species within the Galliformes migrate moderate distances (e.g. white-tailed ptarmigan, *Lagopus leucurus*), have wings of relatively high aspect ratio as well as darker pectoralis muscles (presumably with higher oxidative capacity). This is in contrast with non-migratory species in the clade such as the chukar, which appear to use flight solely for take-off escape from predation risk (Drovetski, 1996; Tobalske and Dial, 2000).

Future directions

Certainly live animals are ideal models for measuring aerodynamic performance, because natural wing flexibility and neuromuscular control of wing movements are far more complex than simple rotation of a dried wing about a fixed shaft. However, because live animals are not suited for measuring performance outside the envelope they will willingly perform, it has been necessary to remove kinematic and neuromuscular variables so that wing form and function may be measured directly. Within this study, wing shape was based off a kinematic analysis of flight in the laboratory and represented standing take-off, vertical flight or slow flight with low advance ratio. At best, the wing posture was relevant to mid-downstroke during flapping flight.

Kinematics of flapping flight are complex, with long-axis rotation of the wings and variation in camber and twist through the wingbeat (Oehme, 1971; Tobalske et al., 2007). It is known from robotic models that unsteady aerodynamics contribute significantly to the forces produced during hovering and slow flight (Ellington et al., 1996; Dickinson et al., 1999; Lehmann, 2004). Recent work using flapping insect wings (Mountcastle and Daniel, 2009) and

computational fluid dynamics (Young et al., 2009) indicates that wing flexibility also has a significant effect upon aerodynamic function. In light of this, it is noteworthy that increasing force coefficients caused greater deformation of the whole wing during spinning (i.e. $\Delta\alpha$ had a positive effect upon C_R), suggesting that aeroelasticity may have deformed the more-developed wings in a manner that increased C_V:C_H (Fig. 2).

Deformation caused a decrease in the absolute value of active α compared with static α, and this has implications for control of flight surfaces. For example, our results indicate that a bird experiencing increased aerodynamic loading on its wings would experience aerodynamic damping of $\Delta\alpha$, which may, therefore, represent a form of passive stability. Increased loading might be initiated passively, due to shifts in wind velocity from turbulence (Combes and Dudley, 2009) or incurrent velocity during maneuvering (Hedrick et al., 2009). Alternatively, increased loading may occur actively, using a muscle such as the supracoracoideus to supinate the wing (Poore et al., 1997; Tobalske and Biewener, 2008).

Overall, then, an important challenge for understanding the effects of dynamic changes in morphology on aerodynamic performance and wing control will be to compare our data representing mid-wing translation with observations of near-field aerodynamics from live animals through the entire wingbeat cycle (e.g. Warrick et al., 2009).

LIST OF SYMBOLS AND ABBREVIATIONS

A	cross-sectional area
C_D	coefficient of profile drag
C_H	coefficient of horizontal force
C_L	coefficient of lift
$C_{L,max}$	maximum coefficient of lift
C_R	coefficient of resultant force
C_V	coefficient of vertical force
d.p.h.	days post hatching
EI	flexural stiffness
E	Young's modulus
F_a	applied force
I	second moment of area
l	effective beam length
Q	air flow
Re	Reynolds number
T	microscale transmissivity
U	wing velocity
U_r	local air velocity
α	active (aerodynamically loaded) angle of attack
δ	feather displacement
ΔP	pressure differential across the feather

ACKNOWLEDGEMENTS

We sincerely thank K. Dial, B. Jackson, D. Carrier and D. Bramble for their assistance in developing, executing and editing this study. We are also grateful to P. Little, who assisted in conceptualizing, engineering and performing the microscale transmissivity experiment. Two anonymous reviewers provided helpful comments on the manuscript.

FUNDING

This research was supported by the National Science Foundation [grants IOS-0923606 and IOS-0919799 to B.W.T.].

REFERENCES

Altshuler, D. L., Dudley, R. and Ellington, C. P. (2004). Aerodynamic forces of revolving hummingbird wings and wing models. *J. Zool.* **264**, 327-332.
Carrier, D. R. (1996). Ontogenetic limits on locomotor performance. *Physiol. Zool.* **69**, 467-488.
Clumpner, C. (1990). Water hardness and waterproofing of oiled birds: lessons from the Pestucca, Exxon Valdez and American trader spills. In *The Effects of Oil on Wildlife: Research, Rehabilitation and General Concern* (ed. J. White and L. Frink), p. 102. Suisun, CA: International Wildlife Rehabilitation Council.
Combes, S. A. and Daniel, T. L. (2003). Flexural stiffness in insect wings. I. Scaling and the influence of wing venation. *J. Exp. Biol.* **206**, 2979-2987.
Combes, S. A. and Dudley, R. (2009). Turbulence-driven instabilities limit insect flight performance. *Proc. Natl. Acad. Sci. USA* **106**, 9105-9108.
Cooke, M. T. (1933). Speed of bird flight. *Auk* **50**, 309-316.
Crandell, K. E. and Tobalske, B. W. (2011). Aerodynamics of tip-reversal upstroke in a revolving pigeon wing. *J. Exp. Biol.* **214**, 1867-1873.
Dial, K. P., Randall, R. J. and Dial, T. R. (2006). What use is half a wing in the ecology and evolution of birds? *Bioscience* **56**, 437-445.
Dial, K. P., Jackson, B. E. and Segre, P. (2008). A fundamental avian wing-stroke provides a new perspective on the evolution of flight. *Nature* **451**, 985-989.
Dial, T. R. and Carrier, D. R. (2012). Precocial hindlimbs and altricial forelimbs: partitioning ontogenetic strategies in mallards (*Anas platyrhynchos*). *J. Exp. Biol.* **215**, 3703-3710.
Dickinson, M. D. (1996). Unsteady mechanisms of force generation in aquatic and aerial locomotion. *Am. Zool.* **36**, 537-554.
Dickinson, M. H., Lehmann, F.-O. and Sane, S. P. (1999). Wing rotation and the aerodynamic basis of insect flight. *Science* **284**, 1954-1960.
Drovetski, S. V. (1996). Influence of the trailing-edge notch on flight performance of galliforms. *Auk* **113**, 802-810.
Ellington, C. P. (1984). The aerodynamics of hovering insect flight. VI. Lift and power requirements. *Philos. Trans. R. Soc. Lond. B* **305**, 145-181.
Ellington, C. P., van den Berg, C., Willmott, A. P. and Thomas, A. L. R. (1996). Leading-edge vortices in insect flight. *Nature* **384**, 626-630.
Frazzetta, T. H. (1975). *Complex Adaptations in Evolving Populations*. Sunderland, MA: Sinauer Press.
Garland, T., Jr and Adolph, S. C. (1994). Why not to do two-species comparative studies: limitations on inferring adaptation. *Physiol. Zool.* **67**, 797-828.
Gould, S. J. and Lewontin, R. C. (1979). The spandrels of San Marco and the Panglossian paradigm: a critique of the adaptationist programme. *Proc. R. Soc. Lond. B* **205**, 581-598.
Hedrick, T. L., Cheng, B. and Deng, X. (2009). Wingbeat time and the scaling of passive rotational damping in flapping flight. *Science* **324**, 252-255.
Heers, A. M., Tobalske, B. W. and Dial, K. P. (2011). Ontogeny of lift and drag production in ground birds. *J. Exp. Biol.* **214**, 717-725.
Jackson, B. E., Segre, P. and Dial, K. P. (2009). Precocial development of locomotor performance in a ground-dwelling bird (*Alectoris chukar*): negotiating a three-dimensional terrestrial environment. *Proc. Biol. Sci.* **276**, 3457-3466.
Lauder, G. V. (1981). Form and function: structural analysis in evolutionary morphology. *Paleobiology* **7**, 430-442.
Lehmann, F.-O. (2004). The mechanisms of lift enhancement in insect flight. *Naturwissenschaften* **91**, 101-122.
Mountcastle, A. M. and Daniel, T. L. (2009). Aerodynamic and functional consequences of wing compliance. *Exp. Fluids* **46**, 873-882.
Müller, W. and Patone, G. (1998). Air transmissivity of feathers. *J. Exp. Biol.* **201**, 2591-2599.
Nice, M. M. (1962). Development of behavior in precocial birds. *Trans. Linn. Soc. N. Y.* **8**, 1-211.
Oehme, V. H. (1971). On the geometrical twist of the avian wing. *Biol. Zentralbl.* **90**, 145-156.
Poore, S. O., Ashcroft, A., Sánchez-Haiman, A. and Goslow, G. E., Jr (1997). The contractile properties of the M. supracoracoideus in the pigeon and starling: a case for long-axis rotation of the humerus. *J. Exp. Biol.* **200**, 2987-3002.
Prum, R. O. (1999). Development and evolutionary origin of feathers. *J. Exp. Zool.* **285**, 291-306.
Rayner, J. M. V. (1988). Form and function in avian flight. *Curr. Ornithol.* **5**, 1-6.
Spedding, G. R., Hedenström, A. and Rosen, M. (2003). Quantitative studies of the wakes of freely flying birds in a low-turbulence wind tunnel. *Exp. Fluids* **34**, 291-303.
Stark, J. M. and Ricklefs, R. E. (1998). *Avian Growth and Development*. New York: Oxford University Press.
Tobalske, B. W. and Biewener, A. A. (2008). Contractile properties of the pigeon supracoracoideus during different modes of flight. *J. Exp. Biol.* **211**, 170-179.
Tobalske, B. W. and Dial, K. P. (2000). Effects of body size on take-off flight performance in the Phasianidae (Aves). *J. Exp. Biol.* **203**, 3319-3332.
Tobalske, B. W. and Dial, K. P. (2007). Aerodynamics of wing-assisted incline running in birds. *J. Exp. Biol.* **210**, 1742-1751.
Tobalske, B. W., Puccinelli, L. A. and Sheridan, D. C. (2005). Contractile activity of the pectoralis in the zebra finch according to mode and velocity of flap-bounding flight. *J. Exp. Biol.* **208**, 2895-2901.
Tobalske, B. W., Warrick, D. R., Clark, C. J., Powers, D. R., Hedrick, T. L., Hyder, G. A. and Biewener, A. A. (2007). Three-dimensional kinematics of hummingbird flight. *J. Exp. Biol.* **210**, 2368-2382.
Tobalske, B. W., Hearn, J. W. D. and Warrick, D. R. (2009). Aerodynamics of intermittent bounds in flying birds. *Exp. Fluids* **46**, 963-973.
Usherwood, J. R. (2009). The aerodynamic forces and pressure distribution of a revolving pigeon wing. *Exp. Fluids* **46**, 991-1003.
Usherwood, J. R. and Ellington, C. P. (2002a). The aerodynamics of revolving wings I. Model hawkmoth wings. *J. Exp. Biol.* **205**, 1547-1564.
Usherwood, J. R. and Ellington, C. P. (2002b). The aerodynamics of revolving wings II. Propeller force coefficients from mayfly to quail. *J. Exp. Biol.* **205**, 1565-1576.
Vogel, S. (1994). *Life in Moving Fluids: The Physical Biology of Flow*. Princeton, NJ: Princeton University Press.
Vogel, S. (2003). *Comparative Biomechanics: Life's Physical World*. Princeton, NJ: Princeton University Press.
Warrick, D. R., Tobalske, B. W. and Powers, D. P. (2005). Aerodynamics of the hovering hummingbird. *Nature* **435**, 1094-1097.
Warrick, D. R., Tobalske, B. W. and Powers, D. R. (2009). Lift production in the hovering hummingbird. *Proc. Biol. Sci.* **276**, 3747-3752.
Withers, P. C. (1981). An aerodynamic analysis of bird wings as fixed aerofoils. *J. Exp. Biol.* **90**, 143-162.
Young, J., Walker, S. M., Bomphrey, R. J., Taylor, G. K. and Thomas, A. L. R. (2009). Details of insect wing design and deformation enhance aerodynamic function and flight efficiency. *Science* **325**, 1549-1552.

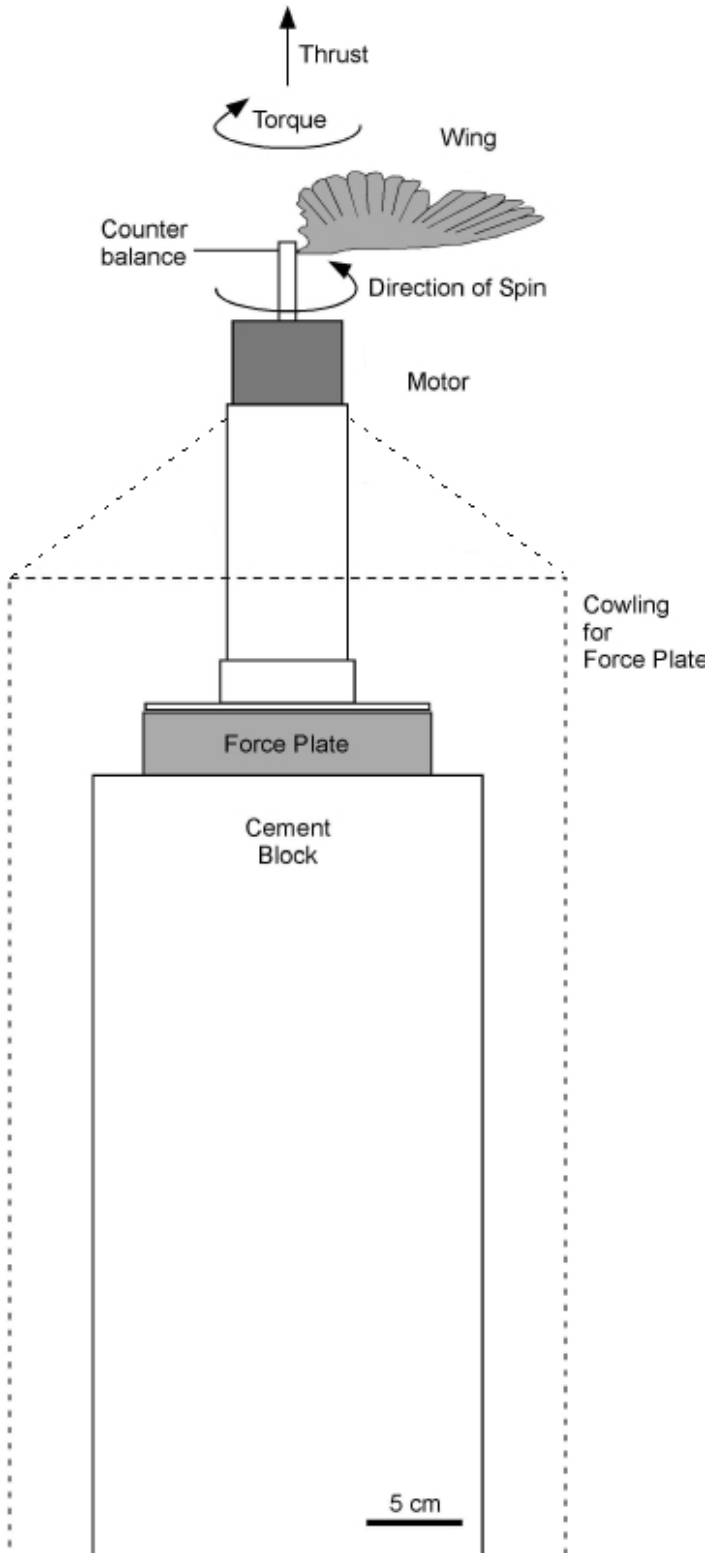

Fig. S1. Experimental setup of propeller–force-plate apparatus. Several motors were interchanged (see Materials and methods) to spin a single wing-mount over both chukar and mallard ontogenetic series at *in vivo* speeds converted to revolutions min^{-1} (Table 1). Force and torque were measured about the *z*-axis and converted into coefficients of lift and drag, respectively. Wings were positioned upside-down and a cowling was placed over the force sensor to reduce the effect of downwash on the force plate readouts.

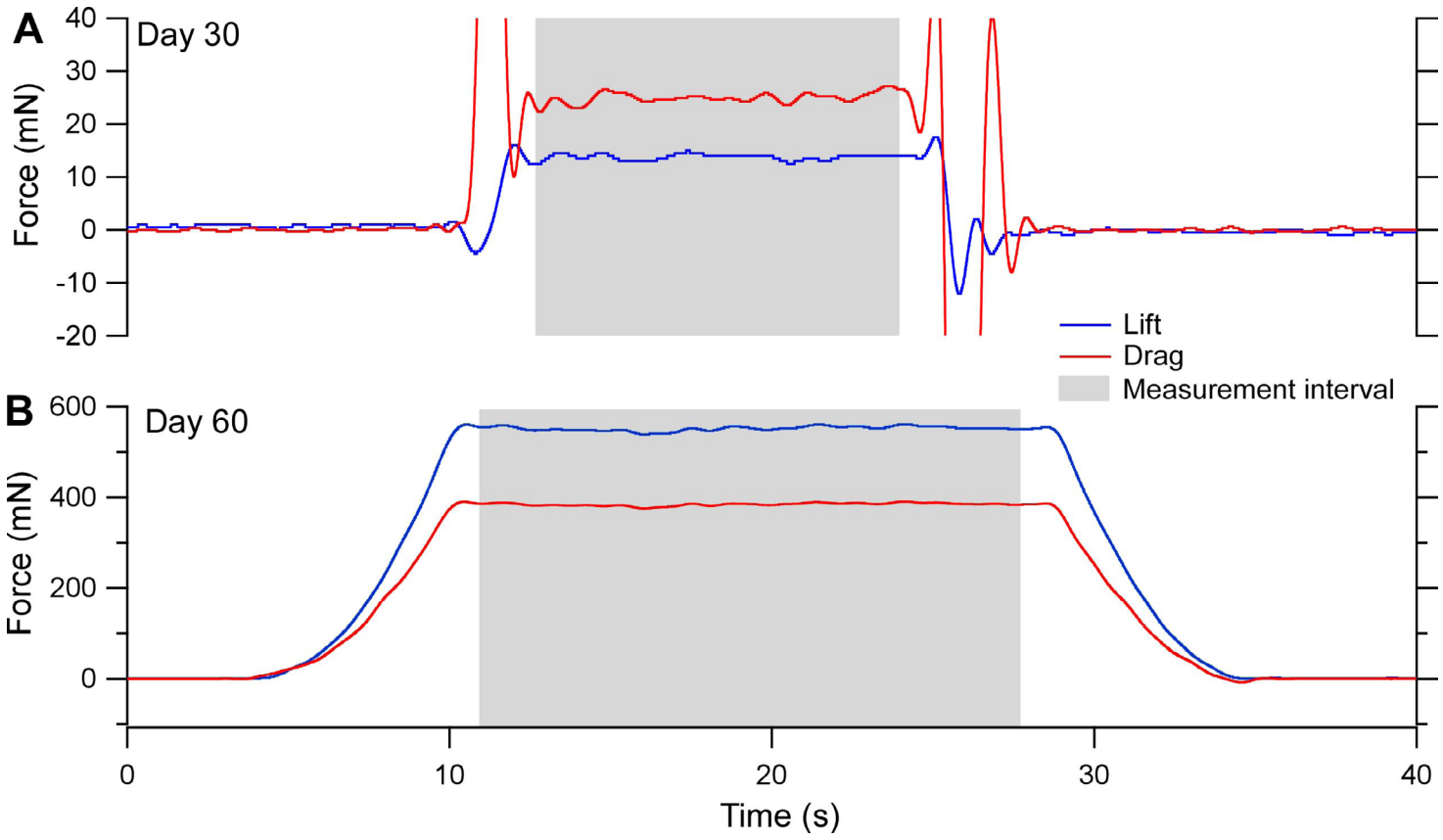

Fig. S2. Force (mN) traces from spinning mallard wings as analyzed using Chart (v.5.2, ADInstruments, Colorado Springs, CO, USA). The raw signals have been filtered using a 1 Hz digital low pass filter. Blue, vertical force, lift; red, horizontal force, drag. Grey indicates the region of data measured during the test. Measurements avoided transient forces at start and stop of activity. Because sample intervals were ≤10 s, the digital filter had no effect upon mean force. (A) Day 30; (B) day 60. The scale in A was chosen for improved resolution for this figure only; torque during motor onset and offset resulted in drag values outside the chosen scale, but data recording was continuous and well within the range of the equipment.

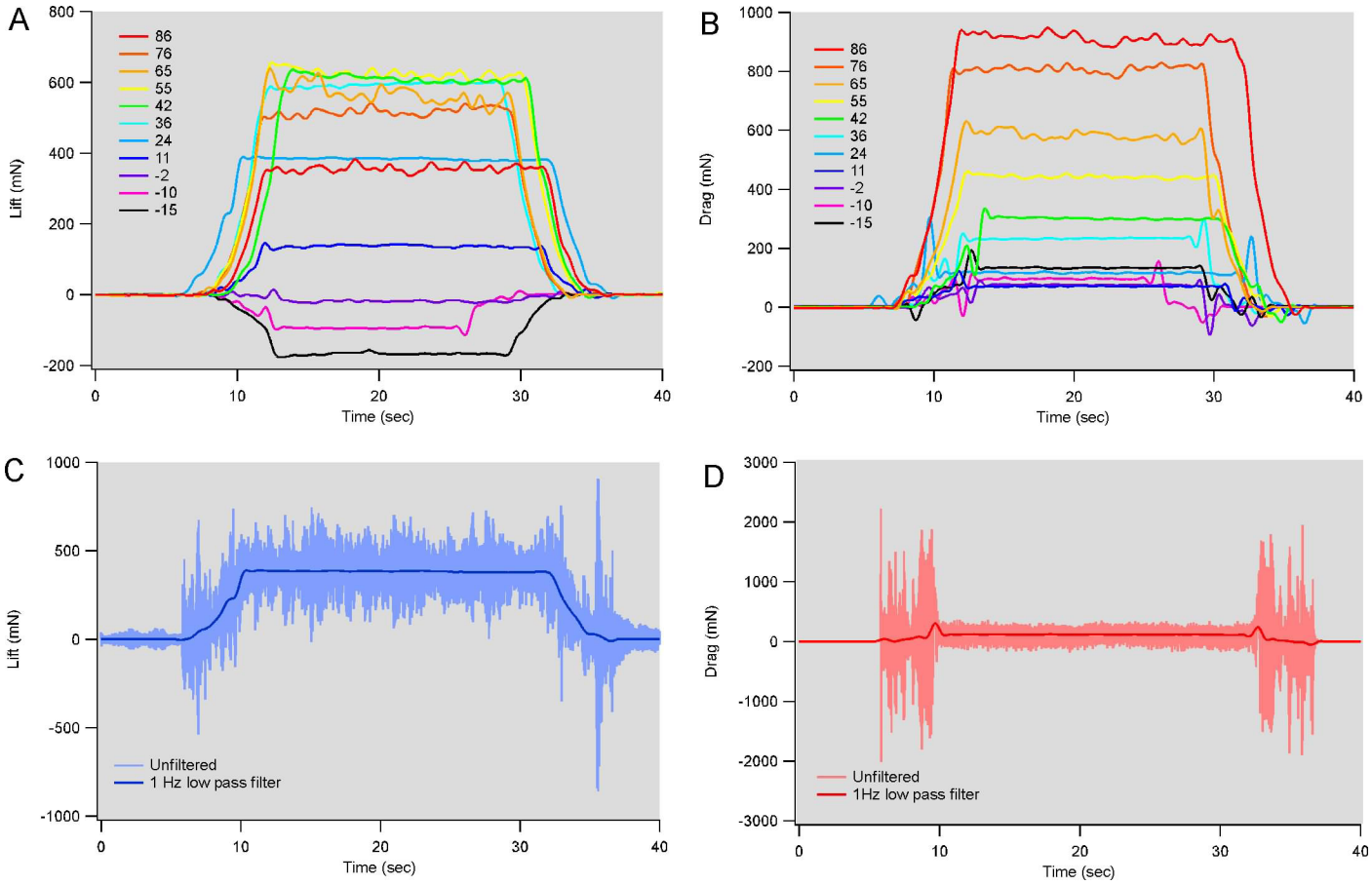

Fig. S3. Raw force plate data are displayed from an individual (day 50) mallard. (A) All signals for lift were filtered at 1 Hz low pass. The key shows the active angle of attack (deg) for each run. (B) All signals for drag were filtered at 1 Hz low pass (key as in A). (C) Lift data for day 50 at 24 deg α (active), showing unfiltered and filtered (1 Hz low pass) data. (D) Drag data for day 50 at 24 deg α (active), showing unfiltered and filtered (1 Hz low pass) data.